On which timescales do gas transfer velocities control North Atlantic CO_2 flux variability?

Matthew P. Couldrey[1], Kevin I. C. Oliver[1], Andrew Yool[2], Paul R. Halloran[3]

and Eric P. Achterberg[1,4]

Key Points:

-Global ocean carbon flux variability is simulated in a general circulation model

-Concentration gradient & transfer velocity control interannual flux variability

-Gas transfer velocity does not control pentadal North Atlantic flux variability

Corresponding author: M. P. Couldrey, University of Southampton, Waterfront Campus, European Way, Southampton, Hampshire, SO143ZH (M.P.Couldrey@soton.ac.uk)

[1]Ocean and Earth Science, University of

Abstract. The North Atlantic is an important basin for the global ocean's uptake of anthropogenic and natural carbon dioxide (CO_2), but the mechanisms controlling this carbon flux are not fully understood. The air-sea flux of CO_2, F, is the product of a gas transfer velocity, k, the air-sea CO_2 concentration gradient, ΔpCO_2, and the temperature and salinity-dependent solubility coefficient, α. k is difficult to constrain, representing the dominant uncertainty in F on short (instantaneous to interannual) timescales. Previous work shows that in the North Atlantic, ΔpCO_2 and k both contribute significantly to interannual F variability, but that k is unimportant for multidecadal variability. On some timescale between interannual and multidecadal, gas transfer velocity variability and its associated uncertainty become negligible. Here, we quantify this critical timescale for the first time. Using an

Southampton, National Oceanography Centre, Southampton, UK

[2]National Oceanography Centre, Southampton, UK

[3]Geography, College of Life and Environmental Sciences, University of Exeter, UK

[4]GEOMAR Helmholtz-Zentrum für Ozeanforschung, Kiel, Germany

ocean model, we determine the importance of k, ΔpCO_2 and α on a range of timescales. On interannual and shorter timescales, both ΔpCO_2 and k are important controls on F. In contrast, pentadal to multidecadal North Atlantic flux variability is driven almost entirely by ΔpCO_2; k contributes less than 25%. Finally, we explore how accurately one can estimate North Atlantic F without a knowledge of non-seasonal k variability, finding it possible for interannual and longer timescales. These findings suggest that continued efforts to better constrain gas transfer velocities are necessary to quantify interannual variability in the North Atlantic carbon sink. However, uncertainty in k variability is unlikely to limit the accuracy of estimates of longer term flux variability.

1. Introduction

Since the onset of the industrial era in the middle of the 18th Century, human activities have altered oceanic and atmospheric chemistry, affecting the climate system. Fossil fuel consumption, changes in land use and cement production rapidly release carbon as carbon dioxide (CO_2) gas from geological reservoirs into the atmosphere, oceans and terrestrial biosphere. This adds large amounts of 'anthropogenic carbon' to the biogeochemically and/or radiatively active 'natural carbon' pool. The effects of CO_2 on the Earth system are numerous and complex, but as a 'greenhouse gas' it is a prominent control on climate [*Myhre et al.*, 2013]. Of the 555 ± 85 petagrams of carbon emitted to the atmosphere between 1750 and 2011 by human activities, about half has remained in the atmosphere while 28% ± 5% has been taken up by the oceans, with the remainder taken up by the terrestrial biosphere [*Ciais et al.*, 2013].

The flux equation, (1), describes the net exchange of CO_2 between the air and the ocean (F). Here, ΔpCO_2 is the disequilibrium between the partial pressures of CO_2 in the air and ocean (pCO_2^{air} - pCO_2^{ocean}). Under this sign convention, an excess of CO_2 in the air gives positive ΔpCO_2 and F, and driving exchange into seawater. If pCO_2^{ocean} is greater, outgassing occurs. pCO_2 in seawater is primarily a function of temperature (T), and dissolved inorganic carbon (DIC), but salinity (S) and alkalinity also affect this. The gas transfer velocity, k, is a parameterization of how several aspects the physical environment enable CO_2 flux. Wind velocity is the main variable affecting k (increasing winds increases k), but ice, surfactants, bubbles and other factors also play important roles [*Wanninkhof et al.*, 2009]. The Schmidt number (the ratio between kinematic viscosity and molecular

diffusion) also affects k, varying with water temperature. α is Henry's constant of CO_2 solubility in seawater [*Weiss*, 1974], quantifying how temperature, salinity and pressure affect solubility.

$$F = \Delta pCO_2 \times k \times \alpha \quad (1)$$

CO_2 flux is difficult to measure directly due to the need for high temporal resolution measurements of $p\mathrm{CO}_2$ and small scale turbulence [*McGillis et al.*, 2001], and so a more common approach is to measure or estimate each quantity on the right hand side (RHS) of equation (1). α is the most straightforward to determine, varying primarily with temperature, but also with salinity. α's contribution to flux variability is generally well-constrained, and found to be minor on interannual timescales (e.g. [*Doney et al.*, 2009]). $\Delta p\mathrm{CO}_2$ and k, however, present distinct challenges for ocean carbon research. The primary challenge with studying global $\Delta p\mathrm{CO}_2$ variability is to place as many measurement systems in as many locations as possible, and to maintain those observations through time. The Surface Ocean CO_2 Atlas (SOCAT) is an example of a global effort to compile measurements of ocean surface CO_2 gathered by autonomous underway systems on commercial vessels and research cruises [*Bakker et al.*, 2014].

The main difficulties in quantifying gas transfer velocity stem from its dependence on several elements of the physico-chemical environment. The main variable used to derive a gas transfer velocity is wind speed, but k is also dependent on the smoothness of the sea surface (i.e. the presence of breaking and non-breaking waves [*Frew et al.*, 2007]), bubble entrainment, rain, buoyancy generated turbulence, surfactants and other factors [*Wanninkhof et al.*, 2009]. Given the large range of variables, and poor constraints of

their effects on k, field measurement of gas transfer velocity is difficult. In attempts to refine these uncertainties, several parameterizations have been proposed, derived using a number of techniques, but there is no consensus which is the most accurate [*Bender et al.*, 2011]. Instead, authors tend to attempt to quantify k uncertainty in two ways: the uncertainty inherent to a particular parameterization (resulting from the spread of datapoints about the polynomial fitted) and the variation in derived k from the use of different parameterizations. Published uncertainties relating to k are often not statistically sound, and represent ad-hoc best estimates of error [*Wanninkhof*, 2014]. The result is that considerable CO_2 flux uncertainty originates from uncertainties in the gas transfer velocity.

While the whole global ocean represents a large net sink of CO_2 for the atmosphere, its uptake is not uniform spatially or temporally. The tropical oceans are net CO_2 outgassing regions, whereas at higher latitudes there is net uptake by seawater [*Takahashi et al.*, 2009; *Landschützer et al.*, 2014]. The major upwelling regions are outgassing zones, and the strongest sites of ocean CO_2 uptake are areas of deep waters formation. In the North Atlantic, the combination of deep water formation and high biological carbon fixation create ideal physical and biogeochemical conditions for strong ocean CO_2 uptake, distinguishing it from other basins [*Sabine et al.*, 2004; *Khatiwala et al.*, 2009]. It is therefore an important focus region in the ocean carbon cycle.

The evolution of the North Atlantic carbon sink on decadal and longer timescales is unclear, yet its quantification is necessary for future climate change prediction [*Halloran et al.*, 2015]. *Bates* [2007] and *Takahashi et al.* [2009] call attention to this gap in knowledge, highlighting that a major limitation to our ability to understand this variability

stems from limited spatiotemporal coverage of CO_2 observations. Although datasets with large spatial coverage exist (e.g. SOCAT [*Bakker et al.*, 2014]), they lack the temporal duration required to study long timescales [*Halloran et al.*, 2015]. Equally, the long time-series sites with sufficient data to quantify multiannual variability, such as the Bermuda Atlantic Time Series (BATS) and others reviewed recently by *Bates et al.* [2014] may not necessarily represent the systems at the basin scale [*McKinley et al.*, 2004]. Given these temporal and spatial data gaps, numerical modelling studies provide unique insight into an incompletely observed system.

It is necessary to understand where observational uncertainties limit our ability to confidently predict future climate change. Previous work investigating global ocean carbon flux interannual variability has found both ΔpCO_2 and k to be important drivers [*Doney et al.*, 2009; *Long et al.*, 2013]. Other work has found that North Atlantic multidecadal CO_2 flux variability is controlled chiefly by the contribution from ΔpCO_2 [*McKinley et al.*, 2011]. Therefore, on these multidecadal timescales, uncertainty in gas transfer velocity variability does not considerably limit estimates of flux variability, because the contribution from k is minor. On some intermediate critical timescale between interannual and multidecadal, flux variability transitions from a regime that is k- and ΔpCO_2-controlled to purely ΔpCO_2-controlled. Presently, neither the magnitude of this critical timescale nor its spatial structure are known, yet both are needed to understand where uncertainties in ΔpCO_2 and k add uncertainty in derived fluxes.

Here, we attribute CO_2 flux variability to contributions from all flux equation components on a range of timescales, to identify the timescales where k becomes unimportant. We hypothesise that on interannual and shorter timescales, both k and ΔpCO_2 will both

be important in controlling flux variability, but that for longer term variability, ΔpCO_2 will be the dominant contributor. We examine 150 years of ocean biogeochemical model output, forced with two scenarios: 1) sharply rising, following historical measurements and RCP 8.5 [*Riahi et al.*, 2011] and 2) fixed preindustrial atmospheric CO_2 concentrations. First, we determine that our setup is appropriate to test our hypothesis, comparing observed and modelled variability. Next, we compare our model's representation of interannual flux variability with those of previous studies, before expanding our methodology to examine more specific timescales of variability. We then identify which long timescales of flux variability, if any, are driven entirely by the ΔpCO_2 contribution, with negligible influence from k. Finally, we examine how successfully one can estimate flux variability with only a very limited knowledge of the contribution of k.

2. Methods

2.1. Model Setup

We investigate the controls of ocean carbon flux variability on different time scales using a numerical ocean general circulation model (GCM); version 3.2 of the Nucleus for European Modelling of the Ocean (NEMO) physical ocean model [*Madec*, 2008]. This model includes sea-ice; version 2 of the Louvain-la-Nueve Ice Model (LIM2, [*Timmermann et al.*, 2005]). NEMO was run with a 1° horizontal resolution using the ORCA-1 grid [*Madec and Imbard*, 1996]. This grid is not sufficient to resolve the mesoscale, but has a finer scale of about 1/3° of latitude at the equator to better represent equatorial upwelling. The grid has 292 × 362 horizontal points and 64 vertical levels (with smaller spacing at the surface, increasing with depth).

NEMO is coupled with an intermediate-complexity ecosystem model, MEDUSA 2.0 [*Yool et al.*, 2013a]. MEDUSA 2.0 separately simulates "large" organisms (mesozooplankton and microphytoplankton like diatoms) and "small" ecosystem members (to represent the microbial loop). MEDUSA 2.0 resolves nitrogen, silicon, iron, carbon, alkalinity and oxygen cycles. The model includes representations of sinking of detrital matter and benthic interactions. The *Nightingale et al.* [2000] gas transfer velocity parameterization is used, with the Schmidt number of *Wanninkhof* [1992]. This parameterization is commonly used as it is considered to be one of the more robust; the function shows a high proportion (82%) the variance of dual-tracer release data explained by wind speed [*Ho et al.*, 2011].

Output from the HadGEM2-ES Earth system model is used as the atmospheric forcing set [*Yool et al.*, 2013b]. HadGEM2-ES includes physical models of the ocean and atmosphere, the terrestrial and ocean carbon cycles, tropospheric chemistry and aerosols [*Collins et al.*, 2011]. The surface fluxes of heat, momentum and freshwater, and atmospheric chemistry from HadGEM2-ES were used to force NEMO at 6-hourly intervals. The atmospheric forcing set for the 'anthropogenic' run prescribes concentrations of atmospheric CO_2 (and other greenhouse gases: methane, nitrous oxide and halocarbons) following RCP 8.5 [*Jones et al.*, 2011]. RCP 8.5 is a high greenhouse gas emissions scenario, with atmospheric pCO_2 exceeding 900ppm by the year 2100 [*Riahi et al.*, 2011] (Figure 1a, green curve). This prescribed anthropogenic source of greenhouse gases into the atmosphere affects the radiative forcing balance and causes a net rise in global temperatures, including Sea Surface Temperature (SST) (Figure 1b). The integration was run for 240 years.

A control run was also generated using a very similar setup to the experimental run, except with a different atmospheric pCO_2 scenario. In this run, atmospheric pCO_2 is held at a preindustrial value of 286 ppmv (Figure 1a, red curve). Only 30 years of this forcing set (i.e. output from HadGEM2-ES run with fixed preindustrial atmospheric CO_2) were available to force NEMO-MEDUSA. Therefore, to obtain a comparable 240 year control run, NEMO-MEDUSA was forced with eight repetitions of the forcing set. The control provides insight into the system's internal variability, without forced changes in the radiation budget (observable in global mean SST: Figure 1, right panel) and global biogeochemistry. Internal variability in the control run on timescales longer than 30 years is evident (e.g. in atmospheric pCO_2 and SST, Figure 1, red curves), but given the forcing setup of this run, it is not included in our analysis.

2.2. Decomposition of CO_2 Flux Variability

To explore the drivers behind CO_2 flux variability, we use a Reynolds decomposition to separate the time-varying (y') and time-mean ($\bar{y}$) components of monthly averaged model output, as in equation (2). The time-varying component is therefore the monthly anomaly from a time mean, representing non-seasonal variability.

$$y = y' + \overline{y} \tag{2}$$

The flux of CO_2 is the product of three variables, equation (1). Therefore, a Reynolds decomposition for three forcing components is needed. The generalised decomposition for three components and its expansion is shown in equations (3-5), where a, b and c are the forcing components, corresponding to the three RHS variables in equation (1).

$$y = abc \tag{3}$$

$$y' + \bar{y} = (a' + \bar{a})(b' + \bar{b})(c' + \bar{c}) \tag{4}$$

$$= \bar{a}\bar{b}\bar{c} + a'\bar{b}\bar{c} + \bar{a}b'\bar{c} + \bar{a}\bar{b}c' + \bar{a}b'c' + a'\bar{b}c' + a'b'\bar{c} + a'b'c' \tag{5}$$

The time-mean component, $\bar{y}$, is time mean of each of the RHS terms in equation (5), as in equation (6). Terms in equation (6) containing the time means of two forcing components ($\overline{a'\bar{b}\bar{c}}$, $\overline{\bar{a}b'\bar{c}}$ and $\overline{\bar{a}\bar{b}c'}$) always have values of zero, giving equation (7).

$$\bar{y} = \overline{\bar{a}\bar{b}\bar{c}} + \overline{a'\bar{b}\bar{c}} + \overline{\bar{a}b'\bar{c}} + \overline{\bar{a}\bar{b}c'} + \overline{\bar{a}b'c'} + \overline{a'\bar{b}c'} + \overline{a'b'\bar{c}} + \overline{a'b'c'} \tag{6}$$

$$= \overline{\bar{a}\bar{b}\bar{c}} + \overline{\bar{a}b'c'} + \overline{a'\bar{b}c'} + \overline{a'b'\bar{c}} + \overline{a'b'c'} \tag{7}$$

We subtract $\bar{y}$ from both sides of equation (5) to solve for the time-varying component of y, equations (8-9). This gives an expression for y' in terms of the contributions from separate components, equation (10). Note that $\overline{\bar{a}\bar{b}\bar{c}} = \bar{a}\bar{b}\bar{c}$, so the difference between the two terms cancels to zero in equation (10).

$$y' = y - \bar{y} \tag{8}$$

$$= (\bar{a}\bar{b}\bar{c} + a'\bar{b}\bar{c} + \bar{a}b'\bar{c} + \bar{a}\bar{b}c' + \bar{a}b'c' + a'\bar{b}c' + a'b'\bar{c} + a'b'c')$$

$$-(\overline{\bar{a}\bar{b}\bar{c}} + \overline{\bar{a}b'c'} + \overline{a'\bar{b}c'} + \overline{a'b'\bar{c}} + \overline{a'b'c'}) \tag{9}$$

$$= a'\bar{b}\bar{c} + \bar{a}b'\bar{c} + \bar{a}\bar{b}c' + (a'b'c' - \overline{a'b'c'}) + (a'b'\bar{c} - \overline{a'b'\bar{c}})$$

$$+(a'\bar{b}c' - \overline{a'\bar{b}c'}) + (\bar{a}b'c' - \overline{\bar{a}b'c'}) \tag{10}$$

We arrive at an equation for flux anomalies by expressing anomalies in the flux equation (1) using the expansion in equation (10):

$$\begin{aligned} F' = & \underbrace{\Delta pCO_2' \bar{k} \bar{\alpha}}_{term1} + \underbrace{\overline{\Delta pCO_2} k' \bar{\alpha}}_{term2} + \underbrace{\overline{\Delta pCO_2} \bar{k} \alpha'}_{term3} + \underbrace{(\Delta pCO_2' k' \bar{\alpha} - \overline{\Delta pCO_2' k' \bar{\alpha}})}_{term4} \\ & + \underbrace{(\Delta pCO_2' \bar{k} \alpha' - \overline{\Delta pCO_2' \alpha' \bar{k}})}_{term5} + \underbrace{(\overline{\Delta pCO_2} k' \alpha' - \overline{\overline{\Delta pCO_2}\ k' \alpha'})}_{term6} \\ & + \underbrace{(\Delta pCO_2' k' \alpha' - \overline{\Delta pCO_2' k' \alpha'})}_{term7} \end{aligned} \tag{11}$$

The physical interpretation of these terms is the anomaly in CO_2 flux from a long term monthly mean produced by variability in ΔpCO_2 (term 1), in k (term 2) and in α (term 3) and through non-linear interactions between components (terms 4 to 7). Rather than consider each of the cross terms (terms 4 to 7) in equation (11) separately, we consider their sum as one term. This is because the role of the cross terms (even when added together) in controlling F' is minor, demonstrated in section 4.1. When summed, the decomposed contributions reliably reconstruct monthly mean fluxes, suggesting that the decomposition is not compromised by covariances between components of the flux equation and synoptic scale variability.

To investigate how much each term in equation (11) contributes to variability in F', we regress the values of terms 1, 2 and 3 at each gridpoint for each month against the monthly flux anomaly at that gridpoint. This method is detailed further by *Doney et al.* [2007] and *Doney et al.* [2009]. For example, to solve for the change in y' due to the first forcing component $a'\bar{b}\bar{c}$, we regress the former against the latter:

$$\frac{\partial y'}{\partial a' \bar{b} \bar{c}} = \beta_a \tag{12}$$

This yields a slope, β, which quantifies how strongly a given RHS term in equation (11) contributes to anomalies in the CO_2 flux. In equation (12), the subscripted a denotes that in this example, β_a signifies the change in y' with respect to variability in the forcing component, a. β close to one indicates that a term contributes strongly to the value of F', whereas a slope of 0 shows that F' is insensitive to that term. Values of β may be less than 0 if a term is anticorrelated with F'. In such cases, one or more terms will have slopes greater than 1 to compensate for a different β being smaller than 0. In general, $\Sigma\beta = 1$ (i.e. the linearity assumption of the regression) does not hold due to cross-correlations, but we find that the sum of all slopes is predominantly in the range $0.8 < \Sigma\beta < 1$. This suggests that the assumption of linearity in the response of y' to its predictors is effectively met.

3. Validation

Previous work has compared output from MEDUSA 2.0 to biogeochemical observations on global and regional scales in more detail [*Yool et al.*, 2013a], which we briefly summarise before elaborating our own validation. In general, the model captures much of the spatial and seasonal patterns of primary productivity, but shows a low bias in the subtropics, a high bias in high nutrient/low chlorophyll regions and underestimates the strength of the North Atlantic spring bloom. MEDUSA 2.0 tends to show 'higher highs' of surface DIC than the GLODAP [*Takahashi et al.*, 2009] fields ([*Yool et al.*, 2013a], their Figure 16), but the broader spatial patterns are well reproduced. Similarly, air-sea ΔpCO_2 seasonal highs and lows are somewhat exaggerated, particularly the North Atlantic winter ([*Yool et al.*, 2013a], their Figures 21 and 22). While these findings are useful to bear in mind,

our study focuses on carbon flux variability on interannual and longer timescales that has not been thoroughly validated.

We first assess the ability of our setup to reproduce the major spatial features of the climatological CO_2 flux by comparing observational time-mean fluxes (the Lamont-Doherty Earth Observatory, or LDEO flux climatology[*Takahashi et al.*, 2009]) with model output (Figure 2). The most prominent large-scale features are well represented in our model: low latitude efflux and high latitude influx. Some of the largest discrepancies between the model and observations occur in the South Pacific, where measurements are sparse. For the purposes of our study, these differences are unimportant, since we focus on the North Atlantic. After interpolating the model North Atlantic CO_2 flux climatology onto the coarser grid of the Takahashi observational climatology, the two can be compared quantitatively. The North Atlantic climatological CO_2 flux is one of the best represented basins in our setup; here, the model somewhat underestimates high values of flux, but otherwise the two are well correlated (with a correlation coefficient r value of 0.80, $p < 0.01$) (Figure 2c).

Next, we attempt to validate the model's temporal variability. Direct CO_2 flux observations representing large spatial and temporal scales do not exist, so instead we validate our model's fCO_2 fields (CO_2 fugacity is almost equivalent to pCO_2, but is scaled for the non-ideal nature of real world gases). We compare our model output against 1) the SOCAT database of surface fCO_2 observations (which maximises spatial coverage at the expense of temporal length) [*Bakker et al.*, 2014] and 2) data collected at the BATS site (to compare variability on the longest timescale possible, although only for a limited area). We compare fields of fCO_2 rather than ΔpCO_2 because in our setup, the atmospheric

247 pCO_2 only varies with the increase prescribed under RCP8.5, and so all of the modelled
248 ΔpCO_2 variability arises from the oceanic side. Spatial and temporal (other than the
249 trend) variability in atmospheric pCO_2 are omitted in our setup, but are small (order
250 1-10ppm) in comparison to the oceanic pCO_2 variability of interest (order 10-100ppm)
251 [*Wanninkhof et al.*, 2013].

252 We compare our model output with $1\times1^\circ$ monthly mean gridded fCO_2 fields from the
253 SOCAT database (version 2) [*Bakker et al.*, 2014]. For this comparison, we first regrid
254 our model output onto the SOCAT grid. Although the dataset includes values from the
255 1970s, the most consistent temporal coverage in the North Atlantic is between 2002 and
256 2011. We chose three locations in zonally distinct regions on the basis that they had the
257 most complete set of observations for this period. We select data from $5\times5^\circ$ degree areas
258 across the North Atlantic (subtropical: northeast of the Carribbean, mid-latitude: east
259 of the Bay of Biscay, and high-latitude: south of Greenland/Iceland) to compare against
260 our model output (Figure 3a, orange boxes). The comparison is insensitive to the exact
261 location of the boxes (shifting their positions by a few degrees gives similar results), and
262 the time period of model output used. It was not possible to apply this comparison to
263 the equatorial Atlantic, as there were insufficient monthly mean fCO_2 values (Figure 3a).
264 We calculate a monthly climatology of time mean fCO_2 fields (Figure 3b, d and f), and
265 monthly anomalies from this climatology for the 2002-2011 period. We then calculate
266 frequency spectra of the fCO_2 anomalies for each box (Figure 3c, e and g). Data gaps
267 were filled with that month's mean value, plus the contribution of the linear trend. Where
268 gaps existed in the SOCAT data, the model output was accordingly subsampled and the
269 resulting gaps were filled in the same way as for the observations.

Clear differences exist between the modelled and observed seasonal cycles of fCO_2 (Figure 3b, d and f). These differences are unimportant for our study, which does not focus on seasonal variability. The comparison between the frequency spectra of the model output and the observations is similar across all boxes: high frequency (short timescale) variability is similar or slightly higher in observations, and low frequencies (long timescales) show slightly more energy in the model. The discrepancies at high frequencies are unsurprising, as the observations will reflect features that are unresolved by the model, such as mesoscale eddies. Although the fCO_2 variability at low frequencies is larger in the model, the agreement with observations is within a factor of 2.

The carbon system data collected at BATS, Bermuda (64° W, 31.5° N), are among the longest and most consistent, covering the years 1991 to 2011. The seasonal cycle amplitudes of all four parameters are well resolved in the model, with systematic offsets in salinity and alkalinity (Figure 4c, e). Non-seasonal variability is well represented (Figure 4b, d, f and h). As with the SOCAT-NEMO comparison, there is substantial high frequency variability in the observations not present in the model output, since the former represents snapshots of real world features, while the latter represents monthly-mean output from a 1×1° model grid cell. Overall, the model tends to underestimate sub-annual variability, but captures the amplitudes on longer timescales that are relevant for this study.

The gas transfer velocity is primarily a function of wind speed, so it is important that our setup reproduces realistic wind fields and variability. Other work has explored the performance of the HadGEM2 models more generally [*Martin et al.*, 2011; *Collins et al.*, 2011]. We compare the wind fields used to force NEMO-MEDUSA with monthly mean

Cross-Calibrated Multiplatform (CCMP) sea surface (10m) winds [*Atlas et al.*, 2011], which cover the period 1988-2011. CCMP zonal wind speed variability is similar to other products' [*Wanninkhof et al.*, 2013], and so our comparison would likely produce similar results if other wind datasets were chosen. We regrid the data from its $0.25\times0.25^\circ$ grid onto a $1\times1^\circ$ grid for comparison with our model output. We construct a monthly climatology and fields of anomalies of wind speeds. Similarly to the other aspects of the validation, we construct frequency spectra of the model and observation anomaly fields (Figure 5). In general, agreement between the model and observations is good for variability with frequencies higher than 0.25 year^{-1}, and somewhat poorer for lower frequencies (longer timescales). In the subpolar and polar North Atlantic, the model underestimates low frequency wind variability.

4. Results

4.1. The roles of flux components in interannual variability

In this section, we investigate the drivers behind interannual CO_2 flux variability, quantifying the contributions of its components, ΔpCO_2, k and α. This approach builds on the methodology of *Doney et al.* [2009], attributing interannual flux variability to each component. First, we establish that our model setup is able to represent CO_2 flux variability comparable to previous estimates using the portion of the simulation which overlaps the observational record.

To assess global CO_2 flux interannual variability, we calculate the root mean square (RMS) or standard deviation of globally integrated monthly flux anomalies. From monthly averaged CO_2 flux fields at each gridpoint, we subtract a long-term mean flux (spanning 1980-2009) for each month to generate anomaly fields. For this time period, variability is

insensitive to the choice of RCP because the scenarios have not yet substantially diverged [*Myhre et al.*, 2013]. We globally integrate those flux anomalies, and calculate the square root of the mean squared anomaly, yielding the RMS. The metric is quite sensitive to the duration over which it is calculated. We calculate the RMS over a similar time period to other studies (1980 to 2009), finding a value of 0.29 Pg C yr^{-1}, comparable previous estimates (Table 1). Two recent observational estimates of interannual flux variability differ by a factor of two ([*Rödenbeck et al.*, 2014] and [*Landschützer et al.*, 2014]), which the authors attribute to differing time periods of study. *Landschützer et al.* [2014] comment that their data do not cover the strong 1997/1998 El Niño period, which made the *Rödenbeck et al.* [2014] estimate much larger.

Qualitatively, our setup captures many of the key regional hotspots of interannual variability between 1980-2009 (Figure 6a): the equatorial Pacific, the subpolar and subtropical oceans, and the south Southern Ocean [e.g. *Doney et al.*, 2009; *Rödenbeck et al.*, 2014]. The North Atlantic is a notable region for its large interannual CO_2 flux variability. The areas with the strongest variability (>1.0 mol m^{-2} yr^{-1}) are in the subpolar gyre, along the sea ice edge of the Labrador Sea, along the Greenland coast and along the path of the North Atlantic Current (NAC). The subtropical gyre shows a relatively moderate level of variability (up to 1 mol m^{-2} yr^{-1}) which decays with distance from the NAC. The equatorial Atlantic shows the lowest overall CO_2 flux variability.

To investigate the causes of the interannual variability illustrated in Figure 6a, we estimate the contribution of each component of the flux equation (1) using the linear expansion of F' (equation (11)). At each grid point for all months, we calculate the contribution of each term in equation (11). Taking each of these contributions, we regress

them against the gridpoint's monthly CO_2 flux anomalies (F') to quantify the influence of that particular term on F', as in equation (12). This allows us to compare the contributions of ΔpCO_2, k, α and the cross terms (Figure 6b-e, respectively) to variability in F'.

Over much the global ocean, ΔpCO_2 is the most important contributor to interannual CO_2 flux variability (Figure 6b), in agreement with the findings of *Doney et al.* [2009]. The global area-weighted mean ΔpCO_2 contribution is 0.20 mol m^{-2} yr^{-1}; about 60% of the global interannual CO_2 flux variability. The role of k is also important in almost all regions, contributing about 35% of global interannual flux variability, but is the most significant where the role of ΔpCO_2 is smaller (6c). Indeed, Figure 6b and c mirror each other, since nearly all interannual variability in the CO_2 flux comes from variability in either ΔpCO_2 or k. This is because the contributions from α and the cross terms are minor (Figure 6d and e). Furthermore, most of the variability observed when considering k and α together as one component comes from k, as was assumed by *Doney et al.* [2009].

Many of the locations where k is an important driver behind interannual CO_2 flux variability coincide with the edges of the seasonally ice-covered oceans. This is because k is scaled by the proportion of each ocean grid cell area that is ice-free. Away from ice edges, k is an important control on F' in such locations as the tropical Pacific and the storm track of the North Atlantic (and to a lesser extent the Pacific). Here, interannual variability in winds is considerable, probably associated with low-frequency modes of climate variability such as the ENSO and the NAO, respectively.

Overall, this analysis yields findings that agree with many of those of *Doney et al.* [2009] insofar as that interannual variability in the global oceanic flux of CO_2 is controlled

primarily by ΔpCO_2, but that k contributes about 40% of this. In the following section, we build upon these findings, exploring the longer multiannual to multidecadal timescales of variability, with an emphasis on the North Atlantic.

4.2. Critical timescale of ΔpCO_2 dominance of CO_2 flux variability

In this section we identify at what time scale, if any, does variability in F become dominated by variability in ΔpCO_2. To explore which parameters dominate flux variability over specific timescales, we average each component's contributions (i.e. $\Delta pCO_2' \bar{k} \bar{\alpha}$ for the contribution of ΔpCO_2, etc.) over various zonal areas to obtain mean contributions on the sub-basin scale. We define zones as polar (Baffin Bay and the Greenland-Iceland-Norwegian, or GIN, Sea), subpolar (60° N-35° N), subtropical (35° N-10° N) and equatorial (10° N-10° S) (Figure 7a). We construct frequency spectra of these zonal mean contributions to quantify the energy of each contribution at specific timescales. Since the contributions from each component are in units of CO_2 flux (mmol m^{-2} d^{-1}), one can compare their magnitudes directly. We also employ Welch's method of segmenting signals to better constrain estimates of the spectra [*Welch*, 1967]. Briefly, this involves segmenting a signal into shorter segments of equal length, calculating the spectra of each segment and then averaging over all segments' spectra to obtain one more robust estimate of the spectrum. In our case, we segment the 150 year series of zonally averaged CO_2 flux anomalies and the contribution from k into 5 non-overlapping segments of 30 year length. This method improves the confidence intervals of the spectrum calculated at the cost of being unable to solve for variability on timescales longer than the segment length. This is because the timescales of interest correspond to the lowest frequencies of variability, and so we plot the spectra in period space to highlight this end of the domain.

Across the North Atlantic, most of the variability in CO_2 flux is attributable to the contribution from either ΔpCO_2 or k; the roles of α and the cross terms are minor (not shown). Therefore, almost all of the spectral energy in CO_2 flux anomalies (Figure 7b-e, blue lines) that does not correspond with the spectrum of k (red) is attributable to the contribution from ΔpCO_2. In other words, where the energy in CO_2 flux anomalies is high, but the energy of k's contribution is lower, most of the discrepancy comes from the contribution of ΔpCO_2. In general, the long period CO_2 flux variability comes from the variability of ΔpCO_2, rather than k. We quantify the CO_2 flux variability that is dominated by the contribution from ΔpCO_2 as being the shortest period of variability where the amplitude of F' variability is at least twice as large as the contribution from k for all longer periods. A factor of two was chosen as it identifies the point at which a clear majority (at least half) of flux variability is attributable to the ΔpCO_2 contribution. To do this, we search along the spectrum from long to short periods for the first period where the spectrum of F' is equal to or less than double the energy of the contribution from k. The vertical dashed lines in Figure 7b-e show the value of this critical timescale for each zonal band. If this number is small, then it means a wider band of long period CO_2 flux variability is controlled entirely by ΔpCO_2.

In the equatorial and subtropical latitudes, a very wide band of long-period variability in CO_2 flux is controlled by ΔpCO_2 (all timescales to the right of the vertical dashed lines in Figure 7c-e). That is to say that the roles of k and α are negligible for these long periods. The same is also true at subpolar latitudes, but the band of timescales is narrower: approximately decadal and longer-term variability in CO_2 flux is almost entirely controlled by ΔpCO_2. The separation of the (95% confidence) error envelopes

around the best estimates of the subpolar, subtropical and equatorial spectra (darker blue and pink lines) indicate that the differences between the spectra at the large-period end are significant. For the polar zone, both ΔpCO_2 and k have an important role in driving flux variability for all timescales longer than interannual (even without curtailing the series length by segmentation), and so there is no long period dominated by ΔpCO_2. In addition to the strong influence of ΔpCO_2, there is also long period variability in k. As k is scaled by sea-ice cover, a negative trend in ice area (in response to a warming climate) will therefore force F' in the long term at high latitudes. Such a decline has been documented in this model setup [*Yool et al.*, 2013b]. Taken over the whole North Atlantic, we find that flux variability on pentadal and longer timescales is greatly dominated by the influence of ΔpCO_2, and k contributes to less than quarter of long period flux variability.

To more fully interpret the spectra of zonally averaged contributions, it is helpful to examine the critical timescale of ΔpCO_2 dominance at each grid point for the anthropogenic run (Figure 8a). At the grid-point scale, one can infer which physical phenomena give rise to the spectra in Figure 7. The polar zone in both runs is dominated by points with no long timescale of ΔpCO_2 dominance: much of Baffin Bay and the western GIN Sea. These regions are strongly influenced by sea ice, but in the eastern ice-free GIN Sea long-period variability is dominated by ΔpCO_2.

The subpolar zone features a soutwest-to-northeast band of gridpoints whose flux variability is only dominated by ΔpCO_2 on multidecadal timescales (higher than elsewhere in the basin). This location coincides with the southern boundary of the NAC. Here, there is long period variability in wind speeds in the model, which drives the critical timescale

of ΔpCO_2 dominance in the subpolar zone ($\sim$10 years) to be longer than the subtropical or equatorial zones ($\sim$3 and $\sim$1 years respectively).

We also estimate the critical timescale using observations in the three locations described in section 3. In the three 5-by-5 degree areas with the largest number of SOCAT monthly mean fCO_2 values, we construct and decompose CO_2 fluxes using these fCO_2 data (as in Figure 3), monthly mean CCMP winds, SST values from the EN4 gridded dataset [*Good et al.*, 2013], and atmospheric pCO_2 from Mauna Loa, Hawai'i [*Thoning et al.*, 2014]. In these locations, there is a sufficient history of ocean fCO_2 data to determine the critical timescale: 2 years in the subtropical box, 0.5 years in the mid-latitude box and 4 years in the high latitude box (values shown as color within black squares in Figure 8a). These values are comparable to those determined using model output in the same locations; 4.6, 3.7 and 4.6 years, respectively.

By examining the same metric for the control run, we can learn the extent to which ΔpCO_2 controls natural variability in the global ocean, without the influence of anthopogenic CO_2 input. For much of the North Atlantic, ΔpCO_2 variability controls most of the CO_2 flux variability in the control run (Figure 8b). Due to the construction of the control run, it is not possible to comment on variability on timescales longer than 30 years, yet this period is sufficiently longer than the ΔpCO_2 critical timescale for most of the ice-free North Atlantic. This means that natural, internal ocean multiannual CO_2 flux variability is quite insensitive to the contribution from k, and therefore that much of the control exerted by the ΔpCO_2 is not purely the product of anthropogenic emissions. In other words, the strong influence of the ΔpCO_2 in many parts of the North Atlantic is naturally occurring, and not purely due to rising atmospheric carbon concentrations.

Such variability in ΔpCO_2 may arise without a rise in atmospheric pCO2 due to ocean circulation (particularly horizontal and vertical advection). Advection acts to reorganise the surface inventories of heat, DIC and alkalinity, thereby modulating ocean pCO_2 [*Doney et al.*, 2009; *Halloran et al.*, 2015].

4.3. CO_2 flux estimation with simplified k

Here, we explore the extent to which flux variability can be reliably estimated in circumstances where we have a minimal knowledge of the variability in gas transfer velocity. In section 1, some of the uncertainties associated with k were outlined. A key question is understanding the extent to which those uncertainties limit our ability to estimate oceanic CO_2 flux variability. We can approximate equation (11) by assuming that variations in the gas transfer velocity (k') and the role of the cross terms (terms 4 to 7) are small (demonstrated in section 4.2). Under these assumptions, terms 2, 4, 5, 6, and 7 vanish, yielding equation (13).

$$F' \approx \Delta pCO_2' \bar{k} \bar{\alpha} + \overline{\Delta pCO_2} \bar{k} \alpha' \tag{13}$$

If these assumptions are valid and equation (13) is a reasonable approximation, the uncertainties associated with k would also become irrelevant in the determination of flux variability. This estimation would be useful in estimating multidecadal flux variability using limited observations, or simple box models. The 'true' simulated CO_2 flux is known in the model, and we are therefore able to determine the error due to the approximation in equation (13). By omitting some contributions, the estimated flux will necessarily have less variability than the actual flux. We therefore assess our estimation by quantifying

469 at each grid point 1) the correlation coefficient (r values) between estimated and model
470 actual fluxes that are significant beyond a level of 95% confidence and 2) the proportion
471 of the flux variability that is captured by the estimation relative to the model's actual flux
472 variability. The error in observational reconstructions of CO_2 flux is likely to differ due
473 to the parameterization of gas transfer in the model, but the model validation (section 3)
474 indicates that the statistical properties of the error should be similar on interannual to
475 decadal timescales.

476 The longest-term variability in the North Atlantic CO_2 flux is primarily controlled
477 by the positive trend in atmospheric pCO_2. Correspondingly, the estimated CO_2 flux
478 correlates very closely with the model's actual series (Figure 9a). However, even without
479 this trend (as in the control run), the actual and estimated fluxes correlate well (Figure
480 9d). In general, the correlations are weaker in the control than in the anthropogenic run,
481 and several local minima are apparent; these also correspond to regions where variability
482 is generally small (Figure 9b and f). The good correlation between estimated and actual
483 fluxes in both the anthropogenic and control runs suggest that the estimation captures
484 the key patterns of flux variability; both anthropogenically and internally driven.

485 In addition to reproducing patterns of flux variability, it is also necessary for the esti-
486 mation to correctly predict magnitudes. Since the estimation omits some contributions,
487 it will naturally show either equal or lower variability than the actual flux. To quantify
488 this, we show the ratio between the estimated and actual modelled CO_2 flux variability
489 (as the RMS of monthly anomalies) (Figure 9c,f). Where the value is 1, the estimation
490 reproduces all the modelled variability; values between 0 and 1 indicate the proportion
491 of variability retained by the estimation. This metric indicates that the estimation is

robust at reproducing most of the modelled variability across the Atlantic, in both the anthropogenic and control runs.

The main area where the flux estimation fares poorly is in the ice-covered North Atlantic. Here, non-seasonal sea ice variability is an important control on fluxes. Our estimation implicitly excludes interannual variability in the ice edge and the multidecadal decline of ice extent, so the fluxes in the region are not well represented. To the south of the NAC there are local minima in correlations and the RMS retained, which are more pronounced in the control run than the anthropogenic. Although these areas are less well estimated than elsewhere in the Atlantic, the variability in these regions is small, and so flux variability on the basin and sub-basin scale will still be well captured.

5. Discussion

Presently, large uncertainties are introduced into calculated CO_2 fluxes via the gas transfer velocity. The choice of wind speed parameterization can vary k by approximately 50% at global mean wind speeds ($\sim$7 m/s) and by 100% at speeds higher than 15 m/s [e.g. *Woolf*, 2005]. The choice of wind product can affect k by 10-40% [*Wanninkhof et al.*, 2002], and variability differs between products [*Wanninkhof et al.*, 2013; *Wanninkhof*, 2014; *Kent et al.*, 2013]. The roles of breaking waves and bubbles are not taken into account when using a purely wind speed-based parameterization of k, so these phenomena introduce poorly constrained uncertainty [*Prytherch et al.*, 2010]. Certainly, these factors all limit our ability to accurately estimate CO_2 flux variability on interannual and shorter timescales, and ongoing work is needed in these areas.

In the high-latitude North Atlantic, the gas transfer velocity controls CO_2 flux variability on longer timescales than elsewhere in the basin. In the regions of the Labrador Sea, Baffin Bay, Denmark Strait and Fram Strait, sea ice cover is an important mediator of gas exchange. Here, long period variability in sea ice cover controls CO_2 flux variability via the gas transfer velocity, since k is scaled by the fraction of area that is ice-free. As a result, there is no long period of variability over which ΔpCO_2 predominantly controls the carbon flux. Therefore, to accurately quantify estimates of the high-latitude North Atlantic carbon flux, a detailed knowledge of sea ice dynamics is necessary.

Over the whole North Atlantic, pentadal and longer-term CO_2 flux variability is dominated by the influence of ΔpCO_2. These longer timescales contrast the shorter, where the role of k is crucial. This suggests that a detailed knowledge of the pentadal to multidecadal control of k on F may not be necessary to quantify the longer term variability of the North Atlantic carbon sink. This finding therefore lends support to the approaches of studies such as that of *McKinley et al.* [2011], which attempt to make judgements about multidecadal variability of the North Atlantic CO_2 sink based purely on pCO_2 observations. In their study, it was found that the oceanic trend in pCO_2 converges to that of the atmosphere when examined over the full 29 year period between 1981 and 2009, but when only decadal timescales are considered the two trends differ. Therefore, if on these same multidecadal timescales, the present day air-sea pCO_2 difference is maintained as *McKinley et al.* [2011] suggest, then the North Atlantic CO_2 sink is approximately stable; neither a decline nor an enhancement of the flux is apparent. Our work would support this approach, since we find the roles of k and α in governing flux variability over this timescale to be minor.

There is a broad increase in the critical timescale with latitude in the North Atlantic, which is explainable in terms of wind speed variability. At the low latitudes, wind speed variability is lower, increasing toward the poles (Figure 5). In addition, mean wind speeds are higher at the poles than the equator, so a given magnitude of wind speed variability at subpolar latitudes will produce greater variability in k than at the equator. This is because k scales with the square of the wind speed in our setup [*Nightingale et al.*, 2000]. This zonal increase in k variability, in addition to the presence of sea ice at the highest latitudes, is what causes the comparable zonal increase of the critical timescale (Figures 7 and 8). Furthermore, wind speed (and hence k) variability is a stronger control on carbon fluxes in the control simulation than the anthropogenic run. This is because the control's fixed atmospheric CO_2 concentration mean there is much less variability in ΔpCO_2 (and therefore also in the CO_2 flux) than in the anthropogenic run. As a result, wind speed variability patterns become relatively more important in setting the critical timescale for the control run than the anthropogenic (Figure 8). This means that k is a more important controller of variability of preindustrial carbon fluxes, although not more important than ΔpCO_2 on pentadal and longer timescales.

Through the comparison of modelled ocean fCO_2 fields against observations from SOCAT and Bermuda, it was shown that our setup underestimates variability on timescales shorter than 1 year. This result is to be expected, since GCMs of this scale will tend not to represent high frequency and small spatial-scale variability well [e.g. *Taylor et al.*, 2012]. This could indicate that the ΔpCO_2 contribution may be a stronger control on fluxes on shorter timescales than our study suggests. Our forcing set underestimates multiannual wind speed variability at high latitudes, which may be associated with an

inability to appropriately represent the NAO (an issue common to many GCMs [*Lee and Black*, 2013]). This could cause the real world critical timescale to be longer than what the model suggests. In the polar zone, the low bias does not affect the critical timescale, since k variability on all timescales is non-negligible. In the subpolar zone, the critical timescale may be underestimated, due to the low bias, yet the observation-derived critical timescales are comparable to the model prediction ($\sim$1-5 years for all three locations, using both model output and observations, Figure 8a).

Current ocean models (including NEMO-MEDUSA) do not derive k from the full range of kinetic factors that control it, and instead parameterize it purely from wind speed. It is likely then, that k variability on interannual and shorter timescales will be underestimated too; since real-world, shorter timescale variability in processes as wave breaking and bubble dynamics etc. is not represented in GCMs. Until a more thorough understanding of the mechanisms underlying k is developed, we will not know exactly how important it is in governing short timescale flux variability. While the unmodeled factors are very likely strong controls on k on short timescales, it is not clear if their variability on longer timescales (decadal and longer) is large, relative to the effect of wind speed. If on these long timescales k variability is dominated by the contribution from wind speed, then wind speed parameterizations of k should be sufficient to estimate decadal gas transfer variability.

It is worth exploring the caveat that we have derived our findings from GCM output. One could expect that other models and configurations would yield slightly different timescales for the emergence of ΔpCO_2 dominance of flux variability. Yet our choice of model and setup appears reliable for the purposes of our study. This experiment has been

shown to produce interannual flux variability comparable to other models as well as observational estimates (Table 1). In addition, it captures real world multiannual fCO_2 variance (Figures 3 and 4) and a reasonable degree of wind speed variability (Figure 5 and [*Lee and Black*, 2013]). Therefore, other models similarly capable of representing multiannual flux, fCO_2 and wind variability would likely give results consistent with those presented here, even if the mechanisms underlying that variability differ. Finally, the choice of gas transfer velocity parameterization can have some effect on the critical timescale derived. Functions [e.g. *McGillis et al.*, 2001] that produce a wider range of k values over the most commonly occurring wind speed range (3 to 15 m/s [*Wanninkhof*, 2014]) impart greater variability into the CO_2 flux, and so would increase the critical timescale. Many of the most commonly used parameterizations, however, show the greatest concordance of derived k values over the range of commonly occurring wind speeds, and so the critical timescale is generally insensitive to the choice of function (see Supporting Information).

While we have clearly identified the roles of each of the components of the flux equation in governing F variability, our methodology only hints at which underlying processes are important. To derive a more complete and mechanistic understanding of the controls on carbon flux variability, further work is necessary. A very broad range of physical, chemical and biological processes cause ocean pCO_2 variability, and so future work should seek to quantify the relative importance of these drivers, while attributing them to specific timescales of variability.

6. Conclusions

We have examined the relative importance of the three components of the air-sea CO_2 flux equation (k, ΔpCO_2 and α) in controlling flux variability on a range of timescales. In the North Atlantic, as for much of the global ocean, we find that sub-annual to interannual variability in ΔpCO_2 and k both have important roles in controlling the air-sea carbon flux, in agreement with previous work (e.g. [*Doney et al.*, 2009]). On these timescales, it is critical to obtain estimates of ΔpCO_2 and k for accurate flux variability to be derived. On pentadal and longer timescales, variability in k is not important, and can be ignored when estimating flux variability. The critical timescale increases from interannual at low latitudes to decadal at high latitudes.

Acknowledgments. The authors are grateful for the input of two reviewers, whose feedback improved the clarity and strength of this manuscript. This work was supported the RAGNARoCC NERC directed research programme (NE/K002546/1, NE/K00249X/1 and NE/K002473/1). The observational data used are available via the relevant references that accompany them in the text. The authors are very grateful to those who have produced and made freely available the CCMP, MLO Atmospheric CO_2, EN4, SOCAT, LDEO Flux Climatology and BATS datasets. The Surface Ocean CO2 Atlas (SOCAT) is an international effort, endorsed by the International Ocean Carbon Coordination Project (IOCCP), the Surface Ocean Lower Atmosphere Study (SOLAS) and the Integrated Marine Biogeochemistry and Ecosystem Research program (IMBER), to deliver a uniformly quality-controlled surface ocean CO2 database. The many researchers and funding agencies responsible for the collection of data and quality control are thanked for their con-

tributions to SOCAT. The model output used in this analysis is available as Supporting Information to this manuscript.

References

Atlas, R., R. N. Hoffman, J. Ardizzone, S. M. Leidner, J. C. Jusem, D. K. Smith, and D. Gombos (2011), A cross-calibrated, multiplatform ocean surface wind velocity product for meteorological and oceanographic applications, *Bulletin of the American Meteorological Society*, *92*(2), 157–174.

Bakker, D., S. Hankin, A. Olsen, B. Pfeil, K. Smith, S. Alin, C. Cosca, B. Hales, S. Harasawa, A. Kozyr, et al. (2014), An update to the Surface Ocean CO_2 Atlas (SOCAT version 2), *Earth System Science Data*, *6*, 69–90.

Bates, N., Y. Astor, M. Church, K. Currie, J. Dore, M. González-Dávila, Melchorález-Dávila, L. Lorenzoni, F. Muller-Karger, J. Olafsson, and M. Santa-Casiano (2014), A time-series view of changing ocean chemistry due to ocean uptake of anthropogenic CO_2 and ocean acidification, *Oceanography*, *27*(1), 126–141.

Bates, N. R. (2007), Interannual variability of the oceanic CO_2 sink in the subtropical gyre of the North Atlantic Ocean over the last 2 decades, *Journal of Geophysical Research*, *112*(C9), C09,013.

Bender, M. L., S. Kinter, N. Cassar, and R. Wanninkhof (2011), Evaluating gas transfer velocity parameterizations using upper ocean radon distributions, *Journal of Geophysical Research: Oceans (1978–2012)*, *116*(C2).

Ciais, P., C. Sabine, G. Bala, L. Bopp, V. Brovkin, J. Canadell, A. Chhabra, R. DeFries, J. Galloway, M. Heimann, C. Jones, C. L. Quéré, R. B. Myneni, S. Piao, and

643 P. Thornton (2013), *IPCC, 2013: Climate Change 2013: The Physical Science Basis.*
644 *Contribution of Working Group I to the Fifth Assessment Report of the Intergovern-*
645 *mental Panel on Climate Change*, chap. 6 Carbon and Other Biogeochemical Cycles,
646 Cambridge University Press.

647 Collins, W., N. Bellouin, M. Doutriaux-Boucher, N. Gedney, P. Halloran, T. Hinton,
648 J. Hughes, C. Jones, M. Joshi, S. Liddicoat, et al. (2011), Development and evaluation
649 of an Earth-System model–HadGEM2, *Geoscientific Model Development*, *4*(4), 1051–
650 1075.

651 Doney, S. C., S. Yeager, G. Danabasoglu, W. G. Large, and J. C. McWilliams (2007),
652 Mechanisms governing interannual variability of upper-ocean temperature in a global
653 ocean hindcast simulation, *Journal of Physical Oceanography*, *37*(7), 1918–1938.

654 Doney, S. C., I. Lima, R. A. Feely, D. M. Glover, K. Lindsay, N. Mahowald, J. K.
655 Moore, and R. Wanninkhof (2009), Mechanisms governing interannual variability in
656 upper-ocean inorganic carbon system and air–sea CO_2 fluxes: Physical climate and at-
657 mospheric dust, *Deep Sea Research Part II: Topical Studies in Oceanography*, *56*(8),
658 640–655.

659 Frew, N. M., D. M. Glover, E. J. Bock, and S. J. McCue (2007), A new approach to
660 estimation of global air-sea gas transfer velocity fields using dual-frequency altimeter
661 backscatter, *Journal of Geophysical Research: Oceans (1978–2012)*, *112*(C11).

662 Good, S. A., M. J. Martin, and N. A. Rayner (2013), EN4: Quality controlled ocean
663 temperature and salinity profiles and monthly objective analyses with uncertainty esti-
664 mates, *Journal of Geophysical Research: Oceans*, *118*(12), 6704–6716.

Halloran, P. R., B. B. B. Booth, C. D. Jones, F. H. Lambert, D. J. McNeall, I. J. Totterdell, and C. Völker (2015), The mechanisms of North Atlantic CO_2 uptake in a large Earth System Model ensemble, *Biogeosciences*, *12*(14), 4497–4508, doi:10.5194/bg-12-4497-2015.

Ho, D. T., R. Wanninkhof, P. Schlosser, D. S. Ullman, D. Hebert, and K. F. Sullivan (2011), Toward a universal relationship between wind speed and gas exchange: Gas transfer velocities measured with 3he/sf6 during the southern ocean gas exchange experiment, *Journal of Geophysical Research: Oceans*, *116*(C4).

Jones, C., J. Hughes, N. Bellouin, S. Hardiman, G. Jones, J. Knight, S. Liddicoat, F. O'Connor, R. J. Andres, C. Bell, et al. (2011), The HadGEM2-ES implementation of CMIP5 centennial simulations, *Geoscientific Model Development*, *4*(3), 543–570.

Kent, E. C., S. Fangohr, and D. I. Berry (2013), A comparative assessment of monthly mean wind speed products over the global ocean, *International Journal of Climatology*, *33*(11), 2520–2541.

Khatiwala, S., F. Primeau, and T. Hall (2009), Reconstruction of the history of anthropogenic CO_2 concentrations in the ocean, *Nature*, *462*(7271), 346–349.

Landschützer, P., N. Gruber, D. Bakker, and U. Schuster (2014), Recent variability of the global ocean carbon sink, *Global Biogeochemical Cycles*, *28*(9), 927–949.

Le Quéré, C., J. C. Orr, P. Monfray, O. Aumont, and G. Madec (2000), Interannual variability of the oceanic sink of CO_2 from 1979 through 1997, *Global Biogeochemical Cycles*, *14*(4), 1247–1265, doi:10.1029/1999GB900049.

Lee, Y.-Y., and R. X. Black (2013), Boreal winter low-frequency variability in CMIP5 models, *Journal of Geophysical Research: Atmospheres*, *118*(13), 6891–6904.

688 Long, M. C., K. Lindsay, S. Peacock, J. K. Moore, and S. C. Doney (2013), Twentieth-
689 Century oceanic carbon uptake and storage in CESM1 (BGC), *Journal of Climate*,
690 *26*(18), 6775–6800.

691 Madec, G. (2008), *NEMO reference manual, ocean dynamic component: NEMO–OPA*, 27,
692 Note du pôle de modélisation, Institut Pierre Simmon Laplace, France, Institut Pierre
693 Simmon Laplace, France.

694 Madec, G., and M. Imbard (1996), A global ocean mesh to overcome the North Pole
695 singularity, *Climate Dynamics*, *12*(6), 381–388.

696 Martin, G. M., N. Bellouin, W. J. Collins, I. D. Culverwell, P. R. Halloran, S. C. Hardiman,
697 T. J. Hinton, C. D. Jones, R. E. McDonald, A. J. McLaren, F. M. O'Connor, M. J.
698 Roberts, J. M. Rodriguez, S. Woodward, M. J. Best, M. E. Brooks, A. R. Brown,
699 N. Butchart, C. Dearden, S. H. Derbyshire, I. Dharssi, M. Doutriaux-Boucher, J. M.
700 Edwards, P. D. Falloon, N. Gedney, L. J. Gray, H. T. Hewitt, M. Hobson, M. R.
701 Huddleston, J. Hughes, S. Ineson, W. J. Ingram, P. M. James, T. C. Johns, C. E.
702 Johnson, A. Jones, C. P. Jones, M. M. Joshi, A. B. Keen, S. Liddicoat, A. P. Lock,
703 A. V. Maidens, J. C. Manners, S. F. Milton, J. G. L. Rae, J. K. Ridley, A. Sellar,
704 C. A. Senior, I. J. Totterdell, A. Verhoef, P. L. Vidale, and A. Wiltshire (2011), The
705 HadGEM2 family of Met Office Unified Model climate configurations, *Geoscientific*
706 *Model Development*, *4*(3), 723–757, doi:10.5194/gmd-4-723-2011.

707 McGillis, W., J. Edson, J. Hare, and C. Fairall (2001), Direct covariance air-sea CO_2
708 fluxes, *Journal of Geophysical Research: Oceans (1978–2012)*, *106*(C8), 16,729–16,745.

709 McKinley, G. A., M. J. Follows, and J. Marshall (2004), Mechanisms of air-sea CO_2
710 flux variability in the equatorial Pacific and the North Atlantic, *Global Biogeochemical*

Cycles, *18*(2).

McKinley, G. A., A. R. Fay, T. Takahashi, and N. Metzl (2011), Convergence of atmospheric and North Atlantic carbon dioxide trends on multidecadal timescales, *Nature geoscience*, *4*(9), 606–610.

Myhre, G., D. Shindell, F. Bréon, W. Collins, J. Fuglestvedt, J. Huang, D. Koch, J. Lamarque, D. Lee, B. Mendoza, T. Nakajima, A. Robock, G. Stephens, T. Takemura, and H. Zhang (2013), *IPCC, 2013: Climate Change 2013: The Physical Science Basis. Contribution of Working Group I to the Fifth Assessment Report of the Intergovernmental Panel on Climate Change*, chap. 8 Anthropogenic and Natural Radiative Forcing, Cambridge University Press.

Nightingale, P. D., G. Malin, C. S. Law, A. J. Watson, P. S. Liss, M. I. Liddicoat, J. Boutin, and R. C. Upstill-Goddard (2000), In situ evaluation of air-sea gas exchange parameterizations using novel conservative and volatile tracers, *Global Biogeochemical Cycles*, *14*(1), 373–387.

Obata, A., and Y. Kitamura (2003), Interannual variability of the sea-air exchange of CO_2 from 1961 to 1998 simulated with a global ocean circulation-biogeochemistry model, *Journal of Geophysical research*, *108*(C11), 3337.

Prytherch, J., M. J. Yelland, R. W. Pascal, B. I. Moat, I. Skjelvan, and M. A. Srokosz (2010), Open ocean gas transfer velocity derived from long-term direct measurements of the CO_2 flux, *Geophysical Research Letters*, *37*(23).

Riahi, K., S. Rao, V. Krey, C. Cho, V. Chirkov, G. Fischer, G. Kindermann, N. Nakicenovic, and P. Rafaj (2011), RCP 8.5—a scenario of comparatively high greenhouse gas emissions, *Climatic Change*, *109*(1-2), 33–57.

Rödenbeck, C., D. C. Bakker, N. Metzl, A. Olsen, C. Sabine, N. Cassar, F. Reum, R. Keeling, and M. Heimann (2014), Interannual sea–air CO_2 flux variability from an observation-driven ocean mixed-layer scheme, *Biogeosciences*, *11*, 4599–4613.

Sabine, C. L., R. A. Feely, N. Gruber, R. M. Key, K. Lee, J. L. Bullister, R. Wanninkhof, C. Wong, D. W. Wallace, B. Tilbrook, et al. (2004), The oceanic sink for anthropogenic CO_2, *Science*, *305*(5682), 367–371.

Takahashi, T., S. C. Sutherland, R. Wanninkhof, C. Sweeney, R. A. Feely, D. W. Chipman, B. Hales, G. Friederich, F. Chavez, C. Sabine, A. Watson, D. C. Bakker, U. Schuster, N. Metzl, H. Yoshikawa-Inoue, M. Ishii, T. Midorikawa, Y. Nojiri, A. Körtzinger, T. Steinhoff, M. Hoppema, J. Olafsson, T. S. Arnarson, B. Tilbrook, T. Johannessen, A. Olsen, R. Bellerby, C. Wong, B. Delille, N. Bates, and H. J. de Baar (2009), Climatological mean and decadal change in surface ocean pCO_2, and net sea-air CO_2 flux over the global oceans, *Deep Sea Research Part II: Topical Studies in Oceanography*, *56*(8-10), 554 – 577, doi:http://dx.doi.org/10.1016/j.dsr2.2008.12.009, surface Ocean CO2 Variability and Vulnerabilities.

Taylor, K. E., R. J. Stouffer, and G. A. Meehl (2012), An overview of CMIP5 and the experiment design, *Bulletin of the American Meteorological Society*, *93*(4), 485–498.

Thoning, K., D. R. Kitzis, and A. Crotwell (2014), *Atmospheric Carbon Dioxide Dry Air Mole Fractions from quasi-continuous measurements at Mauna Loa, Hawaii.*, 2014-08 ed., National Oceanic and Atmospheric Administration (NOAA), Earth System Research Laboratory (ESRL), Global Monitoring Division (GMD), Boulder, Colorado, USA, doi:10.7289/V54X55RG.

Timmermann, R., H. Goosse, G. Madec, T. Fichefet, C. Ethe, and V. Duliere (2005), On the representation of high latitude processes in the ORCA-LIM global coupled sea ice–ocean model, *Ocean Modelling*, *8*(1), 175–201.

Wanninkhof, R. (1992), Relationship between wind speed and gas exchange over the ocean, *Journal of Geophysical Research: Oceans (1978–2012)*, *97*(C5), 7373–7382.

Wanninkhof, R. (2014), Relationship between wind speed and gas exchange over the ocean revisited, *Limnology and Oceanography: Methods*, *12*(6), 351–362.

Wanninkhof, R., S. C. Doney, T. Takahashi, and W. R. McGillis (2002), The effect of using time-averaged winds on regional air-sea CO_2 fluxes, *Gas transfer at water surfaces*, pp. 351–356.

Wanninkhof, R., W. E. Asher, D. T. Ho, C. Sweeney, and W. R. McGillis (2009), Advances in quantifying air-sea gas exchange and environmental forcing, *Marine Science*, *1*.

Wanninkhof, R., G. H. Park, T. Takahashi, C. Sweeney, R. Feely, Y. Nojiri, N. Gruber, S. C. Doney, G. A. McKinley, A. Lenton, C. Le Quéré, C. Heinze, J. Schwinger, H. Graven, and S. Khatiwala (2013), Global ocean carbon uptake: magnitude, variability and trends, *Biogeosciences*, *10*(3), 1983–2000, doi:10.5194/bg-10-1983-2013.

Weiss, R. (1974), Carbon dioxide in water and seawater: the solubility of a non-ideal gas, *Marine Chemistry*, *2*(3), 203–215.

Welch, P. (1967), The use of Fast Fourier Transform for the estimation of power spectra: a method based on time averaging over short, modified periodograms, *IEEE Transactions on Audio and Electroacoustics*, pp. 70–73.

Woolf, D. K. (2005), Parametrization of gas transfer velocities and sea-state-dependent wave breaking, *Tellus B*, *57*(2), 87–94.

779 Yool, A., E. Popova, and T. Anderson (2013a), MEDUSA-2.0: an intermediate com-
780 plexity biogeochemical model of the marine carbon cycle for climate change and ocean
781 acidification studies, *Geoscientific Model Development*, *6*, 1767–1811.
782 Yool, A., E. Popova, A. Coward, D. Bernie, and T. Anderson (2013b), Climate change
783 and ocean acidification impacts on lower trophic levels and the export of organic carbon
784 to the deep ocean, *Biogeosciences*, *10*, 5831–5854.

7. Tables and Figure Captions

Table 1. Comparison of global interannual variability (RMS or Standard Deviation of monthly CO_2 flux anomalies) from various studies

Variability (Pg C yr^{-1})	**Approach**	**Time Period**	**Reference**
0.20	Model	1979-1997	[*Le Quéré et al.*, 2000]
0.23	Model	1961-1998	[*Obata and Kitamura*, 2003]
0.28	Model	1980-1998	[*McKinley et al.*, 2004]
0.34	Model	1979-2004	[*Doney et al.*, 2009]
0.20	Obs and Model	1990-2009	[*Wanninkhof et al.*, 2013]
0.31	Observations	1993-2008	[*Rödenbeck et al.*, 2014]
0.12	Observations	1998-2011	[*Landschützer et al.*, 2014]
0.29	Model	1980-2009	This Study

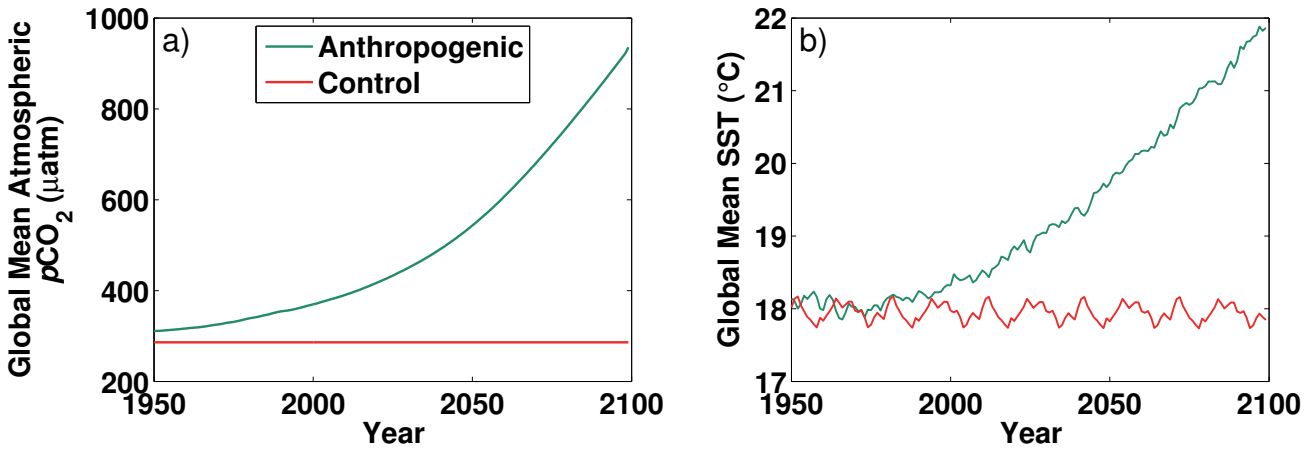

Figure 1. Annual mean atmospheric pCO_2 (a) and Sea Surface Temperature (SST, b) for the anthropogenic (green) and control (red) runs, for 1950-2099 (model year 1 is 1860)

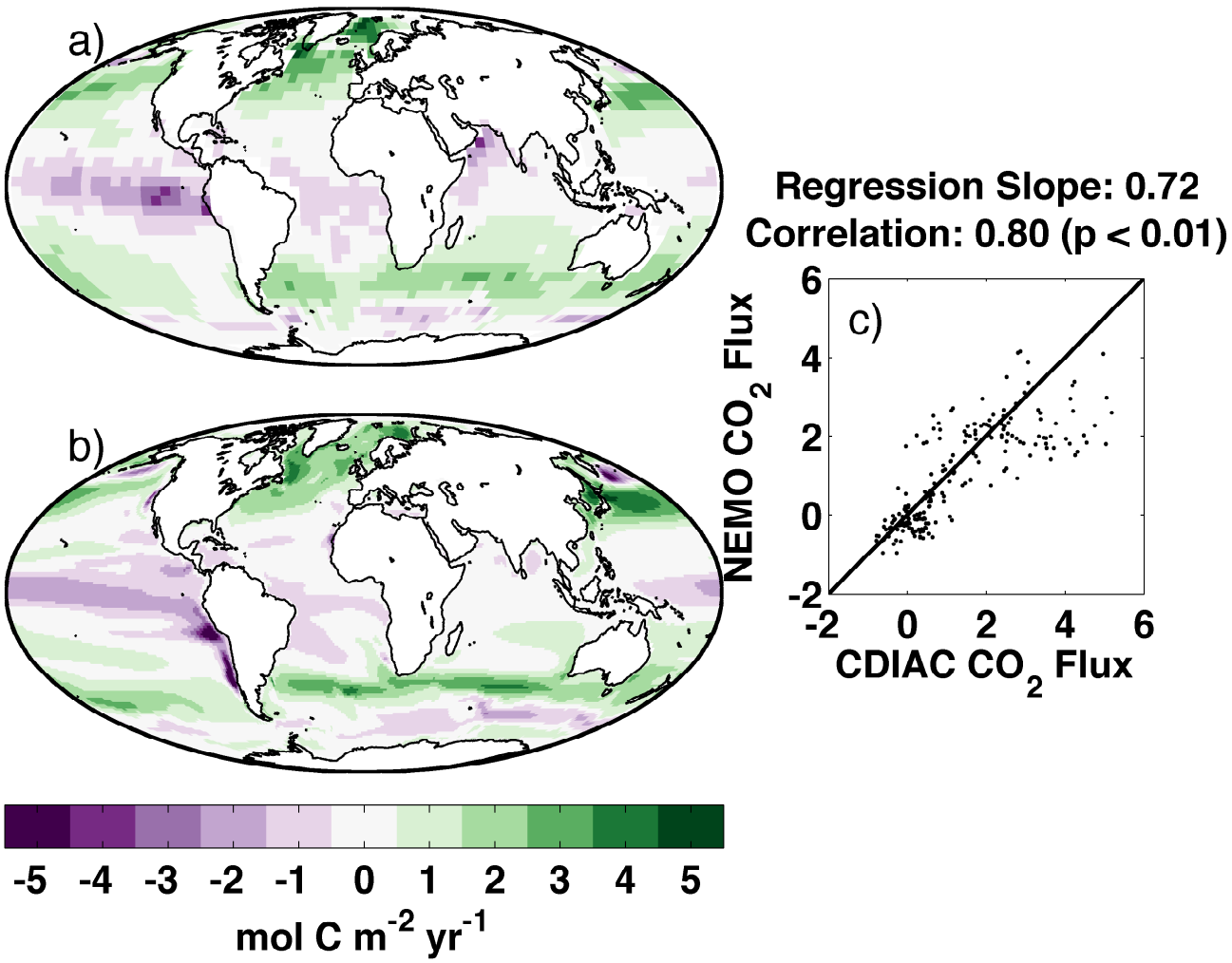

Figure 2. a) LDEO climatological flux of CO_2 into the ocean for the reference year 2000, positive values indicating ocean uptake of gas, [*Takahashi et al.*, 2009], b) Modelled mean CO_2 flux over 1995-2005 for the anthropogenic run, c) LDEO versus modelled North Atlantic climatological CO_2 flux (mol C m^{-2} yr^{-1})

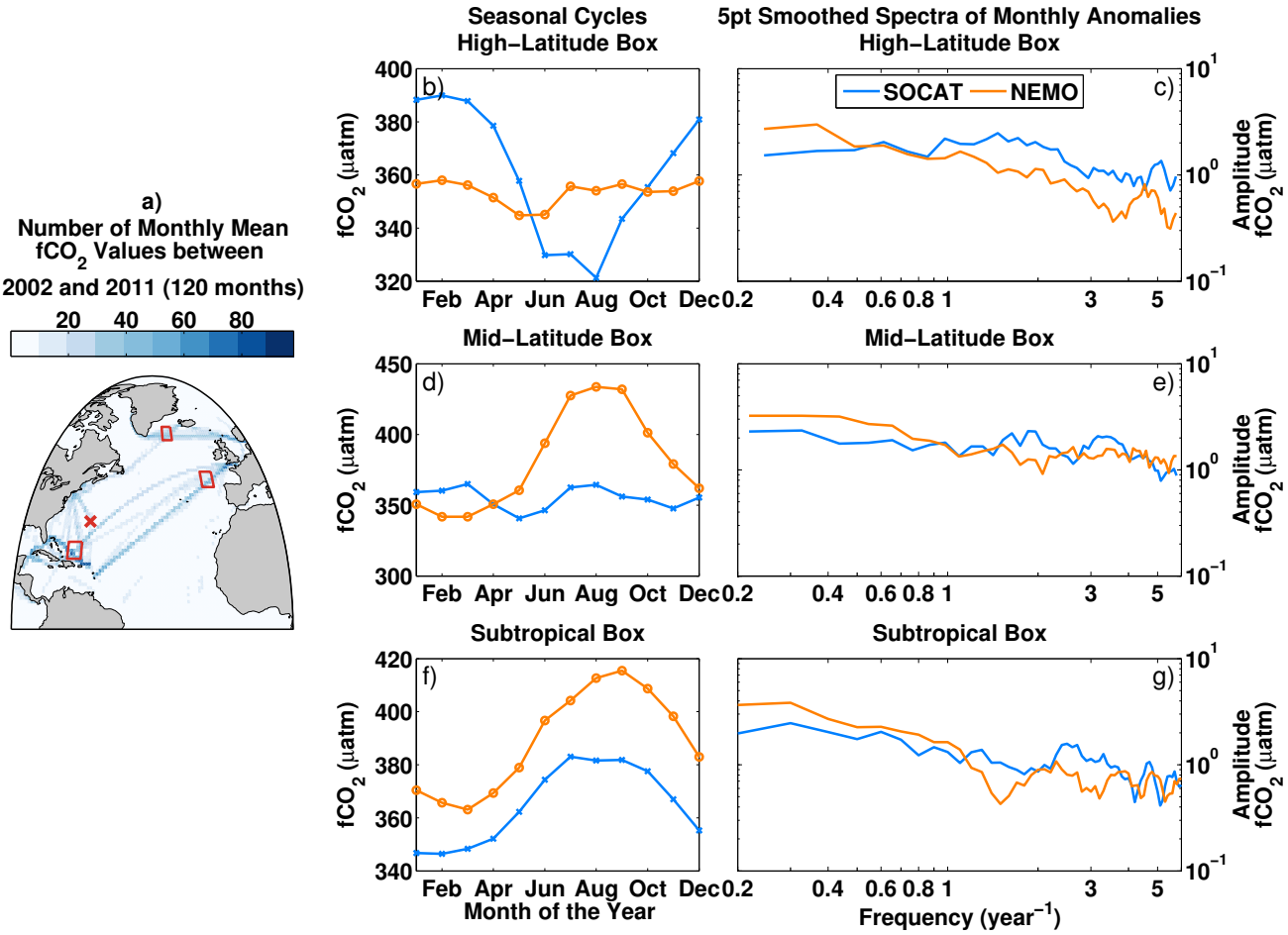

Figure 3. Comparison of data from the SOCAT database and output from the anthropogenic run. a) Coverage of SOCAT monthly mean fCO_2 values 2002-2011, orange squares: locations of comparison regions, orange cross: location of BATS site. b), d) and f), Monthly mean fCO_2 climatologies for the three comparison regions (high-latitude, mid-latitude and subtropical, respectively) for 2002-2011: for SOCAT (blue) and NEMO-MEDUSA (orange). c), e) and g), frequency spectra of monthly fCO_2 anomalies, smoothed with a 5 point running mean

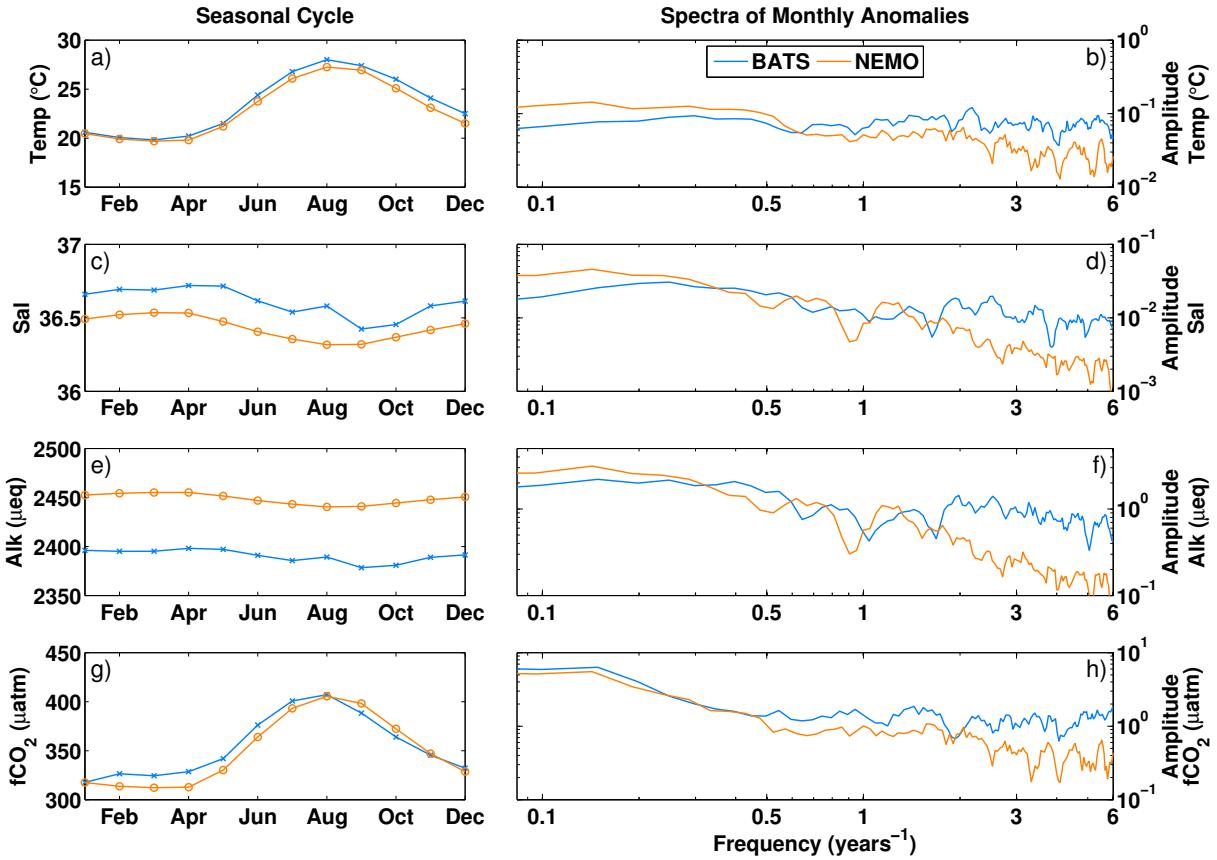

Figure 4. Comparison of (from top to bottom) Temperature, Salinity, Alkalinity and fCO_2 from BATS, Bermuda (blue) with corresponding NEMO-MEDUSA anthropogenic run output (orange). a), c), e) and g), Climatological monthly means for 1991-2011. b), d), f) and h), 5 point smoothed frequency spectra of monthly anomalies for 1991-2011

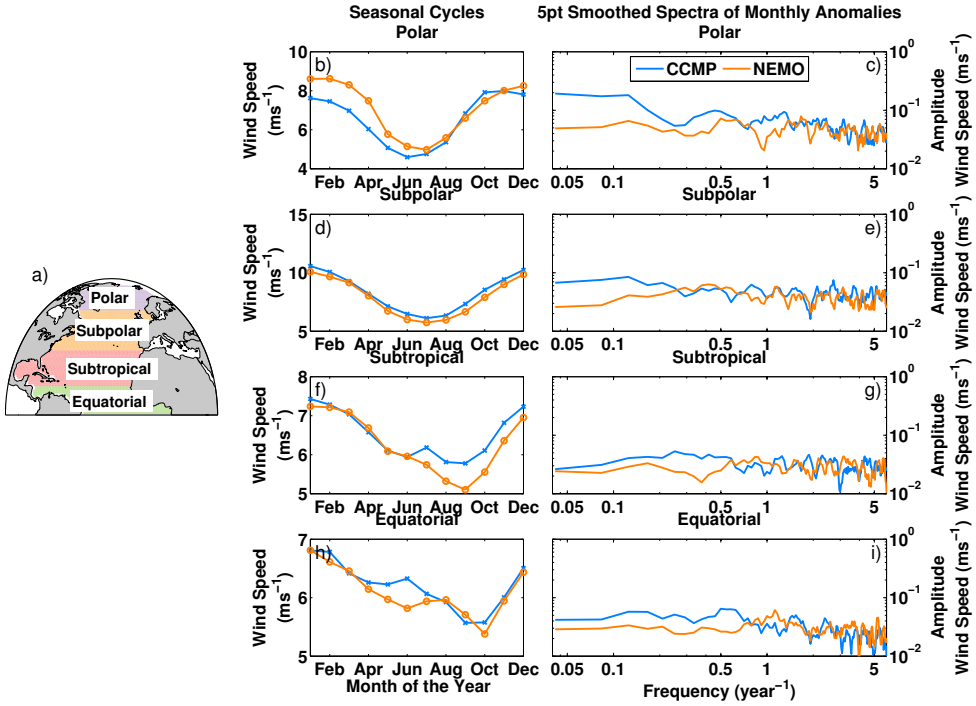

Figure 5. Comparison of wind variability from the CCMP wind product ([*Atlas et al.*, 2011]) and the anthropogenic run. a) Division of zones. b), d), f) and h), Monthly mean wind speed climatologies for the four zonal areas (Polar, Subpolar, Subtropical and Equatorial, respectively) for 1988-2011: for CCMP (blue) and NEMO-MEDUSA (orange). c), e), g) and i), frequency spectra of monthly wind speed anomalies, smoothed with a 5 point running mean

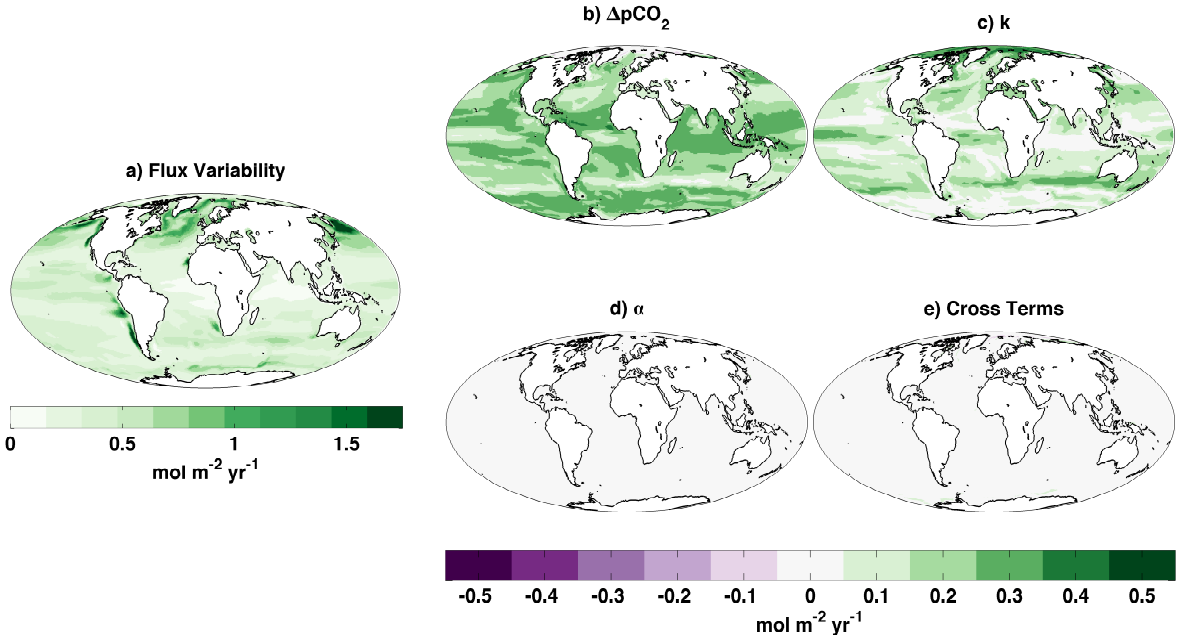

Figure 6. Interannual CO_2 flux variability as the RMS of deseasonalised monthly anomalies (a) and contributions of ΔpCO_2, k, α and cross terms (b to e) to interannual variability in the CO_2 flux for the period 1980-2009 of the anthropogenic run, as in equation (11)

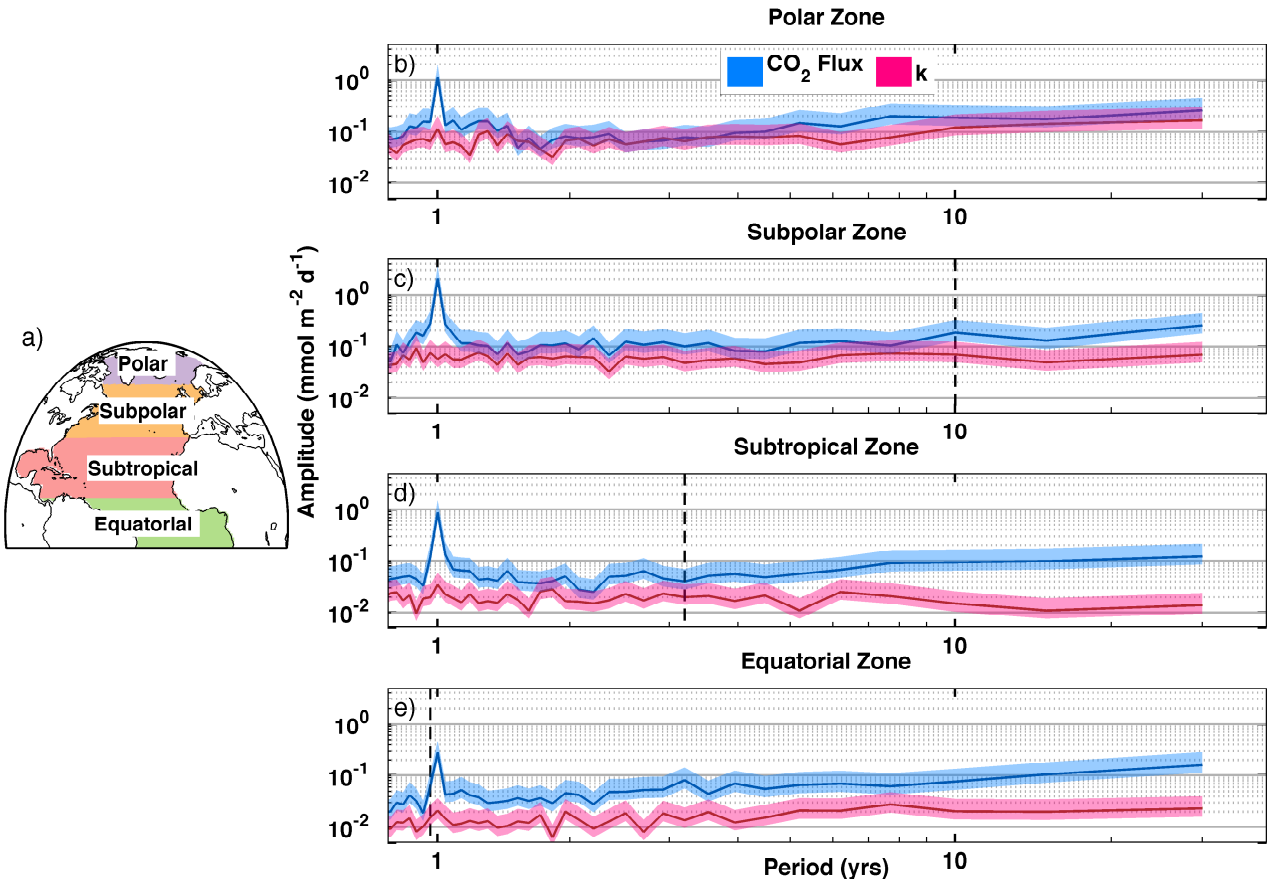

Figure 7. North Atlantic zones (a) and their period spectra of zonally averaged CO_2 flux (blue), and the contribution to flux variability from k (red) for in the anthropogenic run, 1950-2099 (b-e). The dark coloured lines denote best estimates of spectra, lighter shaded regions show the spectra within 95% confidence. Vertical dashed lines indicate the critical timescale: the shortest timescale that for all longer timescales, the best estimate of CO_2 flux variability is at least twice as large as that of k

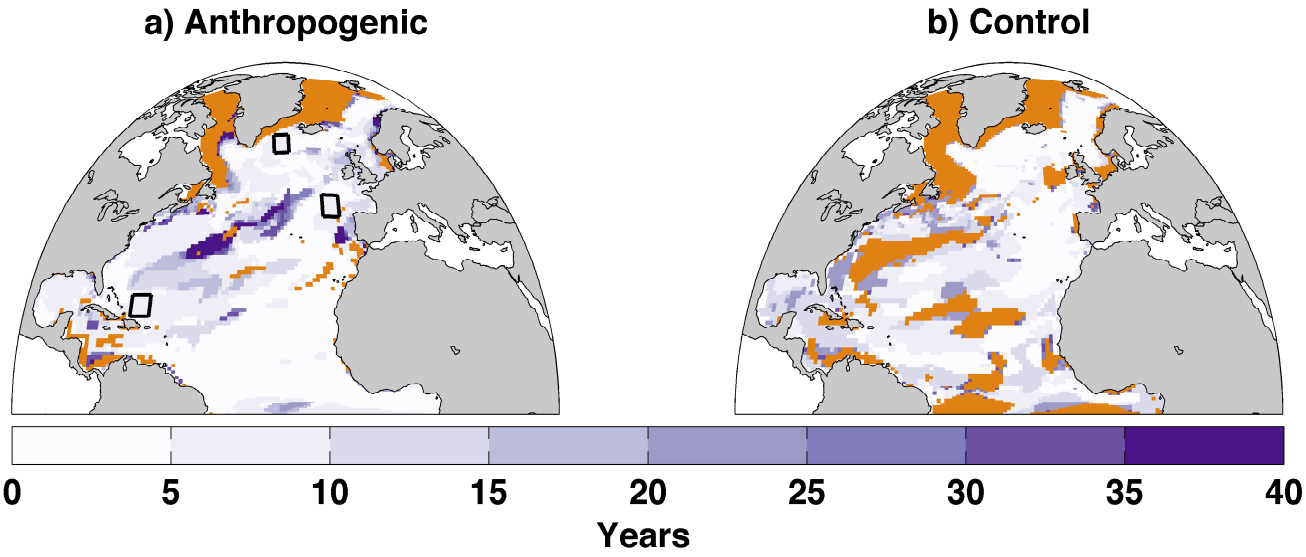

Figure 8. Largest timescale of CO_2 flux variability for which the contribution of k is non-negligible, beyond which variability is dominated by ΔpCO_2 for the anthropogenic (a) and control (b) runs. Shades of purple indicate this timescale, orange areas show where ΔpCO_2 never dominates on the longest timescales and white non-Atlantic areas are out of bounds. Colors inside the three black squares in a) show the timescale derived using observations in the same locations as Figure 3 (CCMP winds [*Atlas et al.*, 2011], SOCAT oceanic pCO_2 [*Bakker et al.*, 2014], MLO atmospheric pCO_2 [*Thoning et al.*, 2014], and EN4 SST [*Good et al.*, 2013])

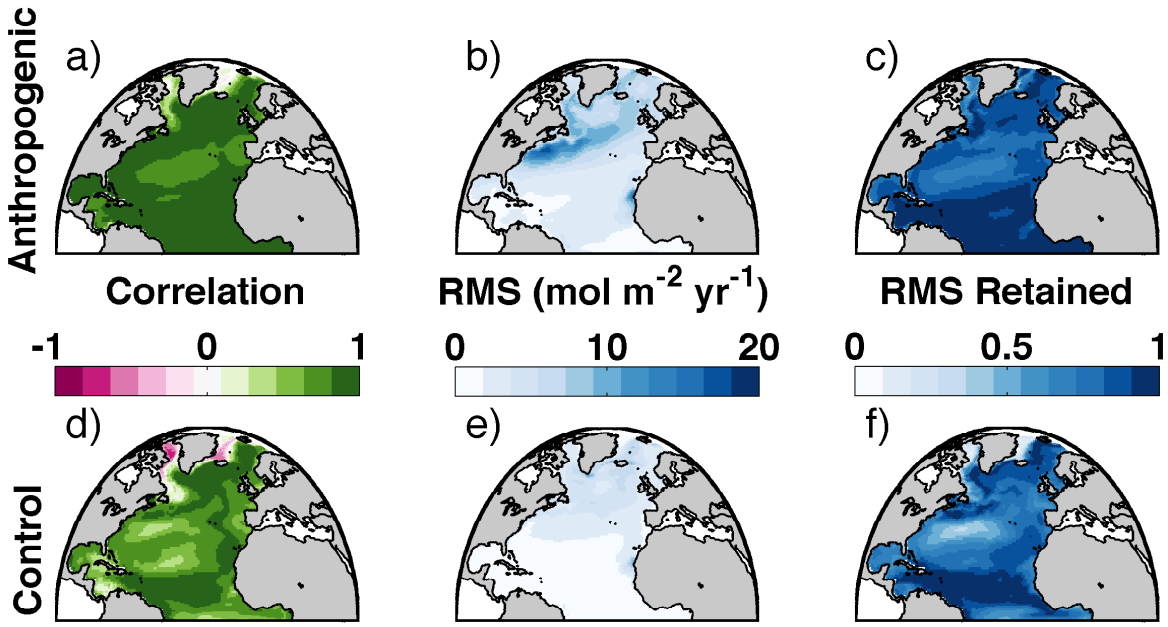

Figure 9. Evaluation of flux estimation applied to the anthropogenic (a-c) and control (d-f) runs, 1950-2099. a) and d), correlation between modelled and estimated fluxes (all values are >95% significance). b) and e), RMS of modelled CO_2 flux anomalies (a measure of variability). c) and f), ratio between estimated and modelled CO_2 flux RMS (the proportion of variability captured by the estimation)